The Effect of Orbital Motions on Synthetic Aperture Radar Imagery of Ocean Waves

WERNER R. ALPERS AND CLIFFORD L. RUFENACH, MEMBER, IEEE

Abstract—The formation of wave-like patterns in synthetic aperture radar (SAR) images of the ocean surface caused by orbital motions is investigated. Furthermore, the degradation in azimuthal resolution due to these motions is calculated by applying a least square fit to the phase history. Formulas are given which describe the variation of intensity in azimuthal direction in the image plane as well as the degradation in azimuthal resolution as a function of ocean wave amplitude, wave frequency, direction of wave propagation, and radar wavelength, incidence angle, and integration time.

I. INTRODUCTION

FOR THE LAST few years there has been considerable interest in imaging ocean waves by synthetic aperture radar (SAR) from aircraft [1]–[6]. More recently with the launch of the oceanographic satellite Seasat-1 on June 26, 1978, SAR images of the ocean have been taken on a daily basis. Though wave-like patterns are discernible on SAR images of the ocean surface obtained from aircraft and Seasat-1, there is still considerable debate on how these images relate to the actual ocean surface wave field [7]–[9].

More fundamentally, it is still controversial as to what physical mechanism is causing the formation of wave-like patterns on SAR images of the ocean surface. For a real aperture radar system the modulation of the radar cross section by the long ocean waves is responsible for the formation of wave images. If the dominant scattering mechanism is Bragg scattering, then this cross-section modulation is attributed to tilt and hydrodynamic modulation [10]. The tilt modulation is due to the change in the local depression angle induced by the long waves, and the hydrodynamic modulation is due to the hydrodynamic interaction between the short Bragg scattering waves and the long waves, which results in a nonuniform distribution of short waves with respect to the long-wave field [10]–[12]. Furthermore, for higher sea states Rayleigh scattering has also been suggested as a candidate for contributing to the cross-section modulation by long ocean waves [4], [8], [12].

For SAR, however, in addition to the cross-section modulation, the orbital motion of the water particles, associated with the long ocean surface waves, can also play a dominant role in the image formation as has been noted by several authors [8], [13], [14]. In this paper we want to investigate in more detail how these orbital motions can produce wave-like patterns in SAR images. The investigation is carried out for a monochromatic deep ocean wave, and we expect that our theoretical results should apply in particular to a swell propagating in the cross-range direction, i.e., in the flight direction. In order to get clearer physical insight into the mechanism causing the image formation, we restrict our analysis to the case $(\omega T/2) < 1$, where ω is the radian frequency of the long ocean wave and T is the radar integration time.

Furthermore, the orbital motions lead to a degradation in azimuthal resolution due to defocusing, which cannot be avoided when imaging ocean waves by SAR. By using a least square fit to the phase history across the aperture we derive this degradation in terms of ocean-wave amplitude, wave frequency, direction of wave propagation, and radar wavelength, incidence angle, and integration time.

II. THEORY

Let us consider a moving target P at the sea surface whose location relative to the radar platform at $t = 0$ is given by the distance in range direction R and by the azimuth or cross-range coordinate x_0 (projection in flight direction). Including the motion of the target, the time history of the return signal is governed by the phase of the scattering amplitude

$$A(t, x_0) = \sqrt{\sigma}\, \exp\left[-j\phi(t, x_0)\right], \tag{1}$$

where

$$\begin{aligned}\phi(t, x_0) &= 2k[(R - \Delta R(t, x_0))^2 \\ &\quad + (Vt - x_0 - \Delta x(t, x_0))^2]^{1/2} \\ &\approx 2k\left[R + \frac{(Vt - x_0)^2}{2R}\right] + \Delta\phi.\end{aligned} \tag{2}$$

$k = 2\pi/\lambda$ is the modulus of the radar wavenumber, V is the ground track velocity of the platform, which is in the x direction, ΔR, Δx are the changes in range and azimuth of the target position due to the motion of the ocean surface, and σ is the cross section associated with the target P. The effect of moving targets on SAR imaging has been treated by Raney [15] who approximated $\Delta R(t)$ and $\Delta x(t)$ by using a Taylor series expansion around $t = 0$ and retaining only terms up to the second order in t. One obtains for the phase perturbation $\Delta\phi$ due to the target motions

$$\Delta\phi = -2k\left[u_r t + \left(\tfrac{1}{2}a_r + \frac{V}{R}u_a\right)t^2\right], \tag{3}$$

where u_r and a_r are the target velocity and acceleration in range direction, respectively, and u_a is the velocity in azimuth direction at $t = 0$. In deriving (3) it has been assumed that $u_a/V \ll 1$. If (3) is applied to ocean waves, however, $Vu_a/R \ll \frac{1}{2}a_r$, and thus the last term can be neglected.

Instead of approximating the phase angle by a Taylor series around $t = 0$, it is more realistic to approximate the phase

Manuscript received October 16, 1978; revised April 11, 1979. This work was supported in part by NATO under Grant SRG10, by the NOAA/NESS Seasat Project, and by the German Science Foundation (DFG, SFB94).

W. R. Alpers was with the Wave Propagation Laboratory, National Oceanographic and Atmospheric Administration, Boulder, CO, and the Jet Propulsion Laboratory, California Institute of Technology, Pasadena, CA, on leave from the Institute for Geophysics and Max-Planck-Institute for Meteorology, Hamburg, Germany.

C. L. Rufenach is with the Wave Propagation Laboratory, National Oceanographic and Atmospheric Administration, Boulder, CO 80302.

0018-926X/79/0900-0685$00.75

error $\Delta\phi$ caused by the motions of the scatterers by a phase error function $\overline{\Delta\phi}$ which provides the best approximation to $\Delta\phi$ in the least square sense across the synthetic aperture with length $L = VT$, where T is the integration time. The approximating function is taken as a second order polynomial of the form

$$\overline{\Delta\phi} = \varphi_0 - 2k(\bar{U}_r t + \tfrac{1}{2}\bar{A}_r t^2), \tag{4}$$

where φ_0 is independent of time. The approximation in the least square sense implies that

$$\int_{-T/2}^{+T/2} (\Delta\phi - \overline{\Delta\phi})^2 \, dt \tag{5}$$

is a minimum. From condition (5) the linear and quadratic coefficients $\bar{U}_r$ and $\bar{A}_r$, respectively, are given by the integrals

$$\bar{U}_r = -\frac{1}{2k}\frac{12}{T^3}\int_{-T/2}^{+T/2} t\Delta\phi(t)\, dt \tag{6}$$

$$\bar{A}_r = -\frac{1}{k}\left[\frac{180}{T^5}\int_{-T/2}^{+T/2} t^2\Delta\phi\, dt - \frac{15}{T^3}\int_{-T/2}^{+T/2}\Delta\phi\, dt\right]. \tag{7}$$

The linear term in t causes a shift of the position of the scatterers in azimuthal direction, while the quadratic term in t gives rise to defocusing in the image plane and thus to a degradation in the azimuthal resolution [2], [7], [16]–[18].

The phase shifts incurred by the motion of the ocean waves are to the first order due to the orbital motions associated with these waves. For deep water waves these motions are circular. The phase change induced by a monochromatic deep water wave with wavenumber $\hat{\mathbf{k}}$, frequency $\hat{\omega}$, and amplitude $\hat{\zeta}_0$ superimposed on a surface current v, which for simplicity is assumed to be time independent, is given by

$$\begin{aligned}\Delta\phi &= -2\int_0^t \mathbf{k}\cdot(\hat{\mathbf{u}}(t') + \mathbf{v})\, dt' \\ &= -2k\hat{\zeta}_0[-\sin\theta\sin\Phi\sin(\hat{\mathbf{k}}\cdot\mathbf{x}_0 - \hat{\omega}t + \delta) \\ &\quad + \cos\theta\cos(\hat{\mathbf{k}}\cdot\mathbf{x}_0 - \hat{\omega}t + \delta)] \\ &\quad - 2k\,|\,\mathbf{v}\,|\cdot t\sin\theta\sin\Phi_c,\end{aligned} \tag{8}$$

where $\hat{\mathbf{u}}$ is the orbital velocity, $\mathbf{k} = (k_x, k_y, k_z) = k(0, \sin\theta, \cos\theta)$ is the radar wavenumber, θ is the incidence angle of the antenna axis ($\theta = 0$ for nadir looking antenna), Φ is the angle between the flight direction and the direction of wave propagation, Φ_c is the angle between the flight direction and the surface current direction, and δ is a constant phase which we choose to be zero. The first term in (8) originates from the horizontal and the second term from the vertical motion of the scatterers. The vertical motion has often been disregarded in the literature [7], [14], but for a large portion of the existing SAR imagery of ocean waves which were taken at incidence angles around 20° (e.g., from the Marineland experiment [2], [3] and the Seasat-1 satellite) it is the dominant term. Inserting (8) into (6) and (7) and integrating over t yields

$$\begin{aligned}\bar{U}_r = \hat{\zeta}_0\hat{\omega}a_1\left(\frac{\hat{\omega}T}{2}\right)&(\sin\theta\sin\Phi\cos\hat{\mathbf{k}}\cdot\mathbf{x}_0 \\ &+ \cos\theta\sin\hat{\mathbf{k}}\cdot\mathbf{x}_0) + v_r\end{aligned} \tag{9}$$

$$\begin{aligned}\bar{A}_r = \hat{\zeta}_0\hat{\omega}^2a_2\left(\frac{\hat{\omega}T}{2}\right)&(\sin\theta\sin\Phi\sin\hat{\mathbf{k}}\cdot\mathbf{x}_0 \\ &- \cos\theta\cos\hat{\mathbf{k}}\cdot\mathbf{x}_0),\end{aligned} \tag{10}$$

where

$$v_r = |\,\mathbf{v}\,|\sin\theta\sin\Phi_c,$$

$$a_1\left(\frac{\hat{\omega}T}{2}\right) = 3\left(\frac{\hat{\omega}T}{2}\right)^{-3}\left[\sin\frac{\hat{\omega}T}{2} - \frac{\hat{\omega}T}{2}\cos\frac{\hat{\omega}T}{2}\right], \tag{11}$$

$$\begin{aligned}a_2\left(\frac{\hat{\omega}T}{2}\right) = 45\left(\frac{\hat{\omega}T}{2}\right)^{-5}&\left[\left(1 - \tfrac{1}{3}\left(\frac{\hat{\omega}T}{2}\right)^2\right)\sin\frac{\hat{\omega}T}{2}\right. \\ &\left. - \frac{\hat{\omega}T}{2}\cos\frac{\hat{\omega}T}{2}\right].\end{aligned} \tag{12}$$

These results are restricted to $\Delta\phi$ variations which can be approximated by a linear and quadratic variation in time. For the harmonic variations of (8) this requires that $(\hat{\omega}T/2) < 1$.

In the limit $\hat{\omega}T/2 \to 0$ we obtain

$$\lim_{\hat{\omega}T\to 0} a_1\left(\frac{\hat{\omega}T}{2}\right) = 1 \tag{13}$$

$$\lim_{\hat{\omega}T\to 0} a_2\left(\frac{\hat{\omega}T}{2}\right) = 1, \tag{14}$$

and thus in this case $\bar{U}_r = u_r + v_r$ and $\bar{A}_r = a_r$, where u_r is the orbital velocity and a_r is the orbital acceleration in the look direction of the antenna at $t = 0$. The functions a_1 and a_2 account for the fact that the perturbation of the phase history caused by the motion of the scatterers is recorded over a finite time interval T.

The average linear and parabolic phase contents of the signal during the integration time T are the more relevant quantities to describe azimuthal displacement and degradation in azimuthal resolution than their values at a fixed time [15]. a_1 and a_2 are plotted in Fig. 1 as a function of $\hat{\omega}T/2$.

The scattering amplitude received by the antenna is weighed by the antenna pattern function which we assume to be Gaussian:

$$G(t, x_0) = \exp\left[-\frac{2(Vt - x_0)^2}{L^2}\right]. \tag{15}$$

In order not to complicate the mathematics we shall ignore here the dependence of the scattering amplitude on range, which is irrelevant for this discussion.

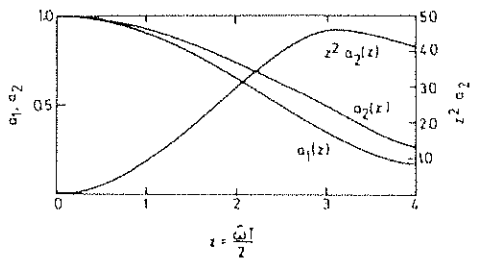

Fig. 1. Plot of a_1 and a_2 defined by (11) and (12) as a function of $z = \hat{\omega}T/2$. Scale for plot is marked on left-hand side. Function $z^2a_2(z)$ is plotted, which appears in (33). Right-hand scale applies to this plot.

SAR processing (see [19] and [20]) includes a dechirping of the received amplitude, which eliminates the quadratic phase term $(Vt)^2/2R$ (see (2)). The dechirping is achieved by applying a matched filter whose transfer function is

$$h(t) = \exp\left[j\frac{k}{R}V^2t^2\right]. \tag{16}$$

This matched filter is adapted to targets having no motions (stationary targets). Thus the scattering amplitude of the target P having a stationary azimuthal coordinate x_0, after applying matched filtering, is given by

$$e(x, x_0) = h^*G \cdot A, \tag{17}$$

where the asterisk denotes convolution in the time domain and $x = Vt$, where x is the azimuthal position of the target in the image plane. In other words, after SAR processing has been applied to the signal, the target, which in case of no motion would be located at x_0, is now located at x. $|e(x, x_0)|^2$ can be calculated by inserting (1), (2), (4), (15), and (16) into (17). As a result one obtains for the power density in the image plane

$$|e(x, x_0)|^2 = \frac{\pi}{2}T^2\sigma(x_0)\frac{\rho_a}{\rho_a'} \cdot \exp\left[-\frac{\pi^2}{\rho_a'^2}\left(x - x_0 - \frac{R}{V}\bar{U}_r\right)^2\right], \tag{18}$$

where

$$\rho_a = \frac{\lambda R}{2VT} \tag{19}$$

is the theoretical azimuthal or Rayleigh resolution for stationary targets (see [15]) and

$$\rho_a' = \rho_a\left\{1 + \left[\frac{4\pi}{\lambda}\left(\frac{T}{2}\right)^2\bar{A}_r\right]^2\right\}^{1/2} \tag{20}$$

is the azimuthal resolution if the target is in motion (defocused resolution). $(4\pi/\lambda)(T/2)^2\bar{A}_r$ is the average parabolic phase error due to target motion and $d_a = \rho_a'/\rho_a$ is called the degradation in azimuthal resolution.

Equation (18) is restricted to phase variations which can be approximated by a linear and quadratic variation with time. For $\hat{\omega}T/2 \gtrsim 1$, (18) is not valid any more. We note that this situation can occur when imaging ocean waves by existing SAR's. However, an analysis of the case $\hat{\omega}T/2 \gtrsim 1$ requires extensive numerical calculations and obscures the insight into the physical mechanism involved. This case is beyond the scope of the present paper and will be considered separately. Furthermore, (18) shows that the true azimuthal position and the apparent azimuthal position of the target in the image, x_0 and x, respectively, do not coincide, but are related by

$$x = x_0 + \frac{R}{V}\bar{U}_r(x_0). \tag{21}$$

The reason for this is that the synthetic aperture radar finds azimuth location via the Doppler coordinate, and the motion of the scatterer in the range direction belies this relation. If the radial velocity component $\bar{U}_r$ is not uniform in azimuth, i.e., if $\bar{U}_r$ is a function of x_0, then the scatterers are shifted in a nonuniform manner in the image plane along the azimuthal direction. Positive and negative $\bar{U}_r$ lead to opposite shifts of the facets in the image plane, thus giving rise to regions which are depleted of scattererrs. More precisely, the backscattered microwave power per unit length in azimuthal direction ("scatter density") varies with x_0 if the radial velocity of the scatterers $\bar{U}_r$ is a function of x_0. The term "velocity bunching" has been used by Larson *et al.* [12] to describe this effect. Assuming that adjacent resolution cells are uncorrelated, see [18], the total power per resolution cell, or the intensity in the image plane $I(x)$, is given by

$$I(x) = \left|\int_{-\infty}^{+\infty} e(x, x_0)\,dx_0\right|^2 = \int_{-\infty}^{\infty}|e(x, x_0)|^2\,dx_0 = \frac{\pi}{2}T^2\int_{-\infty}^{+\infty}\sigma(x_0)\frac{\rho_a}{\rho_a'(x_0)}\exp\left[-\frac{\pi^2}{\rho_a'(x_0)^2}\left(x - x_0 - \frac{R}{V}\bar{U}_r(x_0)\right)^2\right]dx_0. \tag{22}$$

or, after changing the integration variable x_0 to

$$x_0' = x_0 + \frac{R}{V}\bar{U}_r(x_0), \tag{23}$$

by

$$I(x) = \frac{\pi}{2}T^2\int_{-\infty}^{+\infty}\frac{\rho_a}{\rho_a'(x_0)}\frac{\sigma(x_0)}{\left|1 + \frac{R}{V}\frac{\partial}{\partial x_0}\bar{U}_r(x_0)\right|} \cdot \exp\left[-\frac{\pi^2}{\rho_a'(x_0)^2}(x - x_0')^2\right]dx_0'. \tag{24}$$

In order to carry out the integration, the argument x_0 in ρ_a', σ, and $(\partial/\partial x_0)\bar{U}_r$ has to be expressed in terms of x_0' according to (23). If $|1 + R/V\partial\bar{U}_r/\partial x_0|^{-1}$, $\rho_a'(x_0)$ and $\sigma(x_0)$ do not vary very much within the azimuthal resolution cell,

then the integral (24) can be approximated by

$$I(x) \approx \frac{\pi^{1/2}}{2} T^2 \rho_a \frac{\sigma(x_0)}{\left| 1 + \frac{R}{V} \frac{\partial}{\partial x_0} \bar{U}_r(x_0) \right|}. \tag{25}$$

where x_0 must be expressed in terms of x according to (21). For the case where the gradient of the radial velocity component $\bar{U}_r$ in the azimuthal direction varies with x_0, it is evident from this equation that even for a uniform cross section (σ = constant) $I(x)$ will change with x and thus will produce contrast in the image.

III. DISCUSSION

A. Velocity Bunching

The implications of the above desired equations for ocean wave imagery by SAR can now easily be discussed. According to (9) and (21) the shift in azimuth (flight direction) of the scatterer position in the image plane is a harmonic function of x_0. This is illustrated in Fig. 2 for an ocean wave traveling in azimuthal direction ($\Phi = 0$). From this figure it can be seen that the scatter density changes periodically as a function of x_0. The periodicity in azimuth is given by $|\hat{\mathbf{k}}| \cos \Phi$. Thus positive and negative velocity bunchings alternate, which give rise to wave-like patterns in the image film. The scatter density is determined by the azimuthal gradient of the scatterer velocity in range direction $\partial \bar{U}_r / \partial x_0$ (see (24)). We have from (9)

$$\frac{\partial \bar{U}_r}{\partial x_0} = \hat{\xi}_0 |\hat{\mathbf{k}}| \hat{\omega} a_1 \left(\frac{\hat{\omega} T}{2} \right) \cos \Phi [-\sin \theta \sin \Phi \cdot \sin (|\hat{\mathbf{k}}| x_0 \cos \Phi) + \cos \theta \cos (|\hat{\mathbf{k}}| x_0 \cos \Phi)]. \tag{26}$$

$\partial \bar{U}_r / \partial x_0$ is zero for a wave traveling in range direction, but it is not zero for a wave traveling in azimuth. Though the first term (representing the horizontal component of the orbital motion) vanishes in this case the second term (representing the vertical component) does not vanish for $\Phi = \pi/2$. $\partial \bar{U}_r / \partial x_0$ attains its maximum value for small incidence angles θ and for waves traveling in azimuth ($\Phi = 0$). For arbitrary θ and Φ, $\partial \bar{U}_r / \partial x_0$ is proportional to

$$g_1(\Phi, \theta) = \cos \Phi \left[(\sin \theta \sin \Phi)^2 + \cos^2 \theta \right]^{1/2}. \tag{27}$$

Thus velocity bunching is largest for waves traveling in azimuth and vanishes for waves traveling in range direction. We note further that velocity bunching is independent of radar wavelength and that it increases with wave amplitude $\hat{\xi}_0$. In the range $\hat{\omega} T/2 \ll 1$ we have $\partial \bar{U}_r / \partial x_0 \sim \hat{\xi}_0 \lambda^{-3/2}$, while for $\hat{\omega} T/2 \gg 1$ we obtain $\partial \bar{U}_r / \partial x_0 \to 0$. In the latter case velocity bunching disappears in our model since the linear term is a least square fit to a harmonic function which vanishes for large arguments.

The combined effects of velocity bunching and degradation in azimuthal resolution (see 20)) lead to well-defined contrast patterns in the image plane. The relevant quantity is the total power or intensity per azimuthal resolution cell, $I(x)$, which is given by (22). If the variation of $|1 + R/V \partial/\partial x_0 \bar{U}_r|^{-1}$ is within the resolution cell of width ρ_a', i.e., the acceleration $\dot{\bar{U}}_r$ is negligibly small, then from (25) and (26) we obtain

$$I(x)/I_0(x) \approx [1 + c \cos ((|\hat{\mathbf{k}}| x_0 \cos \Phi) + \alpha)]^{-1}, \tag{28}$$

where I_0 is the power per azimuthal resolution cell in the absence of wave motions,

$$c = \frac{R}{V} \hat{\xi}_0 |\hat{\mathbf{k}}| \hat{\omega} a_1 \left(\frac{\hat{\omega} T}{2} \right) g_1(\Phi, \theta), \tag{29}$$

and

$$\alpha = \tan^{-1} (\tan \theta \sin \Phi). \tag{30}$$

c is usually of the order of 10^{-1} (occasionally of the order 1) and thus gives rise to very pronounced contrasts in the image. In Fig. 2 we have inserted a plot of I/I_0 for $c = 0.3$, 0.6, and 0.9 for $\Phi = 0$. Since the wave amplitude of the ocean wave is given by

$$\hat{\xi} = \hat{\xi}_0 \cos (|\hat{\mathbf{k}}| x_0 \cdot \cos \Phi), \tag{31}$$

we observe from (28)–(30) that for azimuthally traveling waves $I(x)$ and $\hat{\xi}$ are out of phase by π. This means that maximum intensity in the image plane is located at the troughs of the wave. For arbitrary θ and Φ the phase shift is given by (30). For c larger than 1 double peaks of $I(x)$ evolve in the interval $0 \leqslant x \leqslant \hat{\lambda}/\cos \Phi$.

If the scale length of $|1 + R/V \partial \bar{U}_r / \partial x_0|^{-1}$ becomes comparable to ρ_a', then the approximation (28) does not hold. The convolution (24) implies that the width of the peaks of $I(x)$ is also determined by ρ_a'. As we will see below, the

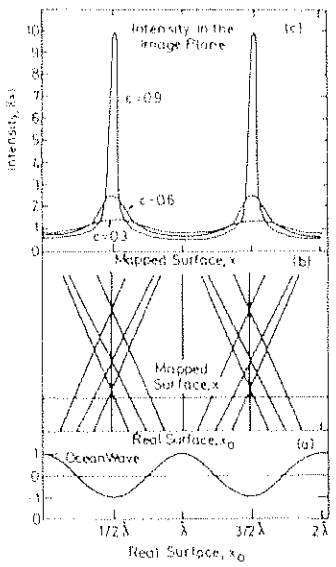

Fig. 2. Illustration of velocity bunching. (a) Surface elevation associated with ocean wave traveling in azimuthal direction. (b) Azimuthal shift of scatterers in image plane. x_0 is azimuthal axis on real surface and x on mapped surface, i.e., in image plane. Shift $x - x_0$ is given by velocity of scatterers in range direction. It is proportional to wave amplitude $\hat{\xi}_0$ and for $\hat{\omega} T/2 \ll 1$ also to wave frequency $\hat{\omega}$. (c) Relative power (intensity) per azimuthal resolution cell as function of azimuthal position x_0 for different values of c defined by (28).

moving target azimuthal resolution ρ_a' increases with radar wavelength if ρ_a is kept fixed. As a consequence, the intensity peaks in the image plane due to velocity bunching become broader for longer radar wavelengths. Thus we expect that velocity bunching can better be seen with radars operating at shorter wavelengths.

Finally, we note that if $R/V\partial\bar{U}_r/\partial x_0 \ll 1$, or, equivalently, $c \ll 1$, we can replace $\alpha\,|\,1 + R/V\partial\bar{U}_r/\partial x_0\,|^{-1}$ in (25) by

$$\alpha' = \alpha\left(1 - \frac{R}{V}\frac{\partial\bar{U}_r}{\partial x_0}\right)\Bigg|_{x_0 \cong x}. \tag{32}$$

With $\partial\bar{U}_r/\partial x_0$ given by (26) one sees that the variation in the cross section due to wave motion is linear in wave amplitude. Thus this variation can be described by a linear modulation transfer function. Therefore, in this case, the results obtained in this paper can be applied to a linear ocean surface wave spectrum.

B. Degradation in Azimuthal Resolution

The azimuthal resolution ρ_a' in the presence of deep ocean waves is given by (20) with $\bar{A}_r$ defined by (10). We can rewrite (20) as

$$d_a = \frac{\rho_a'}{\rho_a} = \left[1 + \left(\frac{4\pi}{\lambda}\hat{\xi}_0\left(\frac{\hat{\omega}T}{2}\right)^2 a_2\left(\frac{\hat{\omega}T}{2}\right) g_2(\theta, \Phi) \cdot \cos(\mathbf{k}\cdot\mathbf{x}_0 + \alpha)\right)^2\right]^{1/2}. \tag{33}$$

where the geometrical function g_2 is given by

$$g_2(\theta, \Phi) = (\sin^2\theta \sin^2\Phi + \cos^2\theta)^{1/2} \tag{34}$$

and the phase α is given by (30). The dependence of d_a on the direction of wave propagation is not very pronounced for most geometries, since $g_2(\theta, \Phi)$ varies between $\cos\theta$ for azimuthally traveling waves and 1 for range traveling waves. The function $((\hat{\omega}T)/2)^2 a_2(\hat{\omega}T/2)$ is plotted in Fig. 1. It can be seen from this plot that for large $\hat{\omega}T/2$ the functional dependence of the parabolic phase error on T deviates considerably from $\sim\hat{\omega}T/2$, which is a consequence of the approximation of the phase error across the aperture by a second order polynominal in a least square sense. Equation (33) shows that for fixed T the degradation in azimuthal resolution decreases with radar wavelength and increases with wave amplitude $\hat{\xi}_0$.

The function a_2 in (33) is approximately 1 for $\hat{\omega}T/2 \lesssim 1$. If we then express T^2 in terms of ρ_a (see (19)) we obtain

$$d_a = \left[1 + \left(\frac{\pi}{4}\left(\frac{R}{V}\right)^2 \hat{\xi}_0\hat{\omega}^2\frac{\lambda}{\rho_a^2} g_2(\theta, \Phi) \cdot \cos(\mathbf{k}\cdot\mathbf{x}_0 + \alpha)\right)^2\right]^{1/2}. \tag{35}$$

This shows that for ρ_a fixed, the degradation in azimuthal resolution increases with radar wavelength λ, ocean wave amplitude $\hat{\xi}_0$, and ocean wave frequency $\hat{\omega}$.

IV. CONCLUSION

The above investigations have shown that the orbital motions associated with ocean surface waves lead to the formation of wave-like patterns in SAR images (velocity bunching) even for a uniform radar scattering cross section as well as to a degradation in radar resolution.

In the present work we have emphasized these orbital motion effects. However, the actual image-forming process for SAR is the combination of two effects:

a) cross section modulation due to the long waves,
b) velocity bunching caused by the orbital motions which is an SAR inherent artifact.

The first effect dominates for waves traveling perpendicular to the flight direction, while the second vanishes in this case and is largest for waves traveling parallel to the flight direction.

For ocean waves traveling at an arbitrary angle both effects compete with each other. Including the degradation in azimuthal resolution, this can lead either to a) a reduction in intensity contrast in the wave image (and eventually to a grey image), b) an enhancement of ocean wave patterns, or c) the occurrence of two (or possibly three) intensity peaks per true wavelength interval (not necessarily equally spaced), depending on the ocean wave and radar parameters.

REFERENCES

[1] W. E. Brown, Jr., C. Elachi, and T. W. Thompson, "Radar imaging of ocean surface patterns," *J. Geophys. Res.*, vol. 81, pp. 2656–2667, 1976.

[2] O. H. Shemdin, W. E. Brown, Jr., F. G. Staudhammer, R. Shuchman, R. Rawson, J. Zelenka, D. B. Ross, W. McLeish, and R. A. Berles, "Comparison of in-situ and remotely sensed ocean waves off Marineland, Florida," *Boundary Layer Meteorol.*, vol. 13, pp. 225–234, 1978.

[3] R. A. Shuchmann, R. R. Rawson, and E. S. Kasischke, "Analysis of synthetic aperture radar ocean wave data collected at Marineland and George Bank," Environment. Res. Inst. Michigan (ERIM), Ann Arbor, MI, 48107, Final Rep.; NOAA Nat. Environment. Satellite Ser. Washington, DC, Contract No. 04-6-158-44078, 1977.

[4] A. Fontanel, "Experiences d'etude de l'etat de la mer par radar lateral," *Actes de Colloques*, no. 5, CNEXO (Brest), pp. 309–326, 1978.

[5] P. G. Teleki, R. A. Shuchman, W. E. Brown, W. McLeish, D. Ross, and M. Mattie, "Ocean wave detection and direction measurements with microwave radar," in *Proc. OCEANS 78*, Washington, DC, Sept. 6–8, 1978.

[6] C. Elachi, "Radar imaging of the ocean surface," *Boundary Layer Meteorol.* vol. 13, pp. 165–1929, 1978.

[7] C. Elachi and D. D. Evans, "Effects of random phase changes on the formation of synthetic aperture radar imagery," *IEEE Trans. Antennas Propagat.*, vol. AP-25, pp. 149–153, Jan. 1977.

[8] C. E. Elachi and W. E. Brown, "Models of radar imaging of the ocean surface waves," *IEEE Trans. Antennas Propagat.*, vol. AP-25, pp. 84-95, Jan. 1977.

[9] R. K. Raney and R. T. Lowry, "Ocean wave imagery and wave spectra distortion by synthetic aperture radar," in *Proc. 12th Int. Symp. on Remote Sensing of Environment*, Manila, pp. 683–702, 1978.

[10] W. C. Keller and J. W. Wright, "Microwave scattering and straining of wind generated waves," *Radio Sci.*, vol. 10, pp. 139–147, 1975.

[11] W. Alpers and K. Hasselmann, "The two-frequency microwave technique for measuring ocean wave spectra from an airplane or satellite", Appendix B, *Boundary Layer Meteorol.*, vol. 13, pp. 215–230, 1978.

[12] W. Alpers and L. Jones, "The modulation of the radar backscattering cross section by long ocean waves," in *Proc. 12th Int. Symp. on Remote Sensing of Environment*, Manila, pp. 1597–1608, 1978.

[13] J. W. Wright, private communication, 1973.

[14] T. R. Larson, L. I. Moskowitz, and J. W. Wright, "A note on SAR imagery of the ocean," *IEEE Trans. Antennas Propagat.*, vol. AP-24, pp. 393–394, May 1976.
[15] R. K. Raney, "Synthetic aperture imaging radar and moving targets," *IEEE Trans. Aerosp. Electron. Syst.*, vol. AES-7, pp. 499–505, 1971.
[16] F. Belanger, "Effect of random phase errors on synthetic arrays," Arizona Electron. Eng. Memo., No. 238, 1966.
[17] F. Belanger, "Parabolic phase errors and defocussing", Goodyear Aerosp. AEEM-373 (Arizona Elec. Eng. Memo.), 1969.
[18] C. T. Swift and L. R. Wilson, "Synthetic aperture radar imaging of ocean waves," submitted to *IEEE Trans. Antennas Propagat.*
[19] R. O. Harger, *Synthetic Aperture Radar Systems.* New York: Academic, 1970.
[20] R. A. Shuchman and J. S. Zelenka, "Processing of ocean wave data from a synthetic aperture radar," *Boundary Layer Meteorol.*, vol. 13, pp. 181–192, 1978.

Werner R. Alpers was born in Hamburg, Germany. He studied physics at the Universities' of Hamburg, Zurich, and Wisconsin. He received the M.S. degree in physics from the University of Wisconsin in 1964 and the Ph.D. degree in theoretical physics from the University of Hamburg, Hamburg, Germany, in 1967.

From 1968 to 1970 he worked in space physics at the European Space Research Institute at Frascati, Italy, and from 1970 to 1973 at the Max-Planck-Institute for Physics and Astrophysics in Munich, Germany. Since 1973 he has been with the University of Hamburg, and the Max-Planck-Institute for Meteorology in Hamburg, Germany, working on radio oceanographic research problems. His current research activities are focused on measuring ocean surface waves and currents using active microwave sensors.

Clifford L. Rufenach (S'62–M'70) was born in Ronan, MT, in 1936. He received the B.S. and M.S. degrees from Montana State University, Bozeman, in 1962 and 1963 and the Ph.D. degree from the University of Colorado, Boulder, in 1971, all in electrical engineering.

From 1963 to 1966 he worked on radio propagation problems at the Stanford Research Institute and from 1967 until present he has been working for the Environmental Research Laboratories of the National Oceanographic and Atmospheric Administration (NOAA), Boulder, CO. His work at NOAA includes research on the radio physics of the ionosphere and interplanetary medium and, more recently, on remote sensing of the ocean surface using satellite and aircraft sensors.

Dr. Rufenach is a member of Tau Beta Pi, Sigma Xi, the American Geophysical Union, and URSI.

Synthesis of Antenna Arrays with Spatial and Excitation Constraints

N. BALAKRISHNAN, P. K. MURTHY, AND S. RAMAKRISHNA

Abstract—Synthesis of antenna arrays subject to spatial and excitation constraints to yield arbitrarily prescribed patterns in both the mean-squared and minimax sense are discussed. The spatial constraints may require that the interelement spacings be greater than a prescribed value or that the element locations lie within a specified region. The excitation constraints are of the form where the current-taper ratio is constrained to be less than or equal to a prescribed value. The technique employed consists of reducing the constrained optimization problem into an unconstrained one by the use of simple transformations of the independent variables. In such cases where explicit transformations are not available, a created response surface technique (CRST) has been used to convert the constrained optimization problem into a series of unconstrained optimizations. The optimization has been carried out using a nonlinear simplex algorithm. Numerical examples are given wherein both the linear and circular arrays are synthesized subject to constraints.

Manuscript received July 6, 1978; revised February 27, 1979.
The authors are with the Department of Aeronautical Engineering, Indian Institute of Science, Bangalore 560 012, India.

I. INTRODUCTION

THE PROBLEM of synthesizing nonuniformly spaced antenna arrays has been studied quite extensively, and comprehensive accounts of the techniques employed have appeared in books [1], [2]. These techniques include the Fourier series expansion, methods of approximation theory, and interpolation.

Very few attempts have been made where synthesis has been carried out subject to constraints on element positions, currents, or pattern characteristics such as sidelobe level or beamwidth. Schuman and Strait [3] have described an iterative approach to synthesize arrays whose elements are constrained to lie within specified limits. Sandrin, Glatt, and Hague [4] have reported a method employing a computerized multivariate search technique wherein constraints on sidelobe levels, beamwidths, and interelement spacings may be imposed. Perini [5] has employed the steepest descent technique to design arrays with large interelement spacings. Schjaer-Jacobson and Madsen [6] have described a nonlinear minimax

0018-926X/79/0900-0690$00.75